Effect of Silver Addition on Transient and Steady State Creep Characteristics of Eutectic Sn-9Zn Binary Alloy

M. Y. Salem

Physics Department, Faculty of Science at New Valley, Assuit University, 72511, El-Kharga, Egypt
Email: mahmoud_salem569@yahoo.com

Transient, and steady state creep characteristics of Sn-9Zn lead-free solders and Sn-9Zn-2Ag ternary alloy was investigated in the temperature range from 323 to 403 K near the transformation temperatures at different five stresses ranged from 3.62 to 11.22 MPa. Both alloys showed improvement in the creep parameters n and β. The value of n and β are higher in ternary than in binary. The activation energies of transient creep of Sn-9Zn binary and Sn-9Zn-2Ag ternary alloy have been found to be 20.16:28.82 kJ/mole and 14.01:20.22 kJ/mole, in low and high temperature range. The relationship through steady-state creep rate ε'_{st} *and the stress* σ *is* $\varepsilon'_{st} = C\sigma^m$ *wherever* $m=(\partial \ln \varepsilon'_{st}/\partial \ln \sigma)$*, is the strain rate sensitivity parameter. This exponent is raised with rising T and* σ *in both alloys. The activation energies of* steady *creep of Sn-9Zn binary and Sn-9Zn-2Ag ternary alloy have been found to be 21.99:24.73 kJ/mole and 15.13:22.07 kJ/mole, in low and high temperature zones respectively. Addition of small amount of Ag (2%) to the binary alloy raised its creep behaviour and ductility and was found to be enhancing the plasticity of the ternary alloys. This behaviour was attributed to the formation of inter metallic compounds (IMCs)* Ag_3Sn *during solidification. Micro-structural variations were studied by Optical microscope (OM), and X-ray diffraction.*

1. Introduction

Universal interests over the environmental effect and health influences of Pb-based solders in used electronics have guide to the development of Pb-free solder substitutional. Among these lead- free solders, Sn-9Zn-2Ag ternary alloy is one of the candidates for the replacement of the Pb-rich solders, which has been extensively used in electronic packaging [1].

Sn-9Zn-2Ag is prepared to be more suitable for higher temperature applications such as step soldering technology, flip-chip connection [2–4] and solder ball connections [5].

For employment wanting dimensionally constant solders, a minimum creep

rate is wanted. Noticing that creep conductance of Sn-9Zn based solders is one of the pre-requisites for behaviour of these solders in the industrialization of electronic products. Since the alloy is aimed to employments at high temperatures. In this study creep mechanisms, play a significant role because of high identical temperatures involved. Furthermore, creep properties of the alloy are influenced by a number of operator such as phase morphology, phase dimensions, presence of Ag as solid solution in the matrix or its precipitation as Ag_3Sn and grade of ageing [1].

The creep resistance of the alloy rely on the volume fraction of the rigid inter metallic compound (IMCs) phases and the distortion resistance of such precipitates through creep [6]. The Ag additions have been reported to improve the microstructure of Sn-9Zn alloys and ductility [7]. The purpose of the present work is to study the effects of addition of small amounts of Ag (2%) on the microstructure and creep properties of Sn-9Zn lead-free solder alloys. Hopefully, these small element additions can play a positive role in the improvement of the overall mechanical properties of the Sn-9Zn based alloys. The consequences are interest useful in the further exploitation of recent solder alloys for different electronic packaging employment.

2. Experimental Procedures

In the present work, description of the microstructure and creep behaviour was achieved on Sn-9Zn lead-free solder alloys and Sn-9Zn-2Ag with the compositions (wt.%) of Sn-9Zn, and Sn-9Zn-2Ag as seen in Table (1). The lead-free solders were prepared from Sn, Zn, and Ag (purity 99.97%) as raw materials. The method of melting was achieved in a vacuum arc furnace under high purity argon atmosphere to output bar-like specimen with a radius of approximately 7 mm. The melt was stay at 500°C for 60 min to complete the dissolution of Sn, Zn, and Ag then poured in a steel mould to get ready the chill cast ingot. A cooling rate of 6-8 °C/s was done, in order to produce the accurate microstructure typically found in few solder joints in microelectronic packages.

A solution of 2% HCl, 3% HNO_3 and 95% (vol.%) ethyl alcohol was prepared and used to etch the samples. Phase identification of the used samples accomplished out by X-ray diffractometry (XRD) at 40 KV and 20 mA using Cu Kα radiation with diffraction angles (2θ) from 20.99◦ to 99.99◦ and a stationary scanning speed of 1°/min. The solder ingots were then mechanically machined into a wire samples with a gauge length equal 5 cm for each samples.

To get samples including the completely precipitated phases and free from any plastic strain aggregation during machining, the samples were annealed at 130° C for 1 hour, then left to cool quietly to room temperature. Tensile tests were achieved with a tensile testing machine, waiting time of 5 min for the test temperatures to be arrived. The used chamber temperature could be spotted by

utilized a thermocouple touching with specimen.

Table (1): Actual compositions of the experimental alloys, wt.%..

Experimental alloys	Sn	Zn	Ag
Sn-9Zn	91	9	0
Sn-9Zn-2Ag	89	9	2

2. Results and Discussion

3.1. Features of Creep Curves

3.1.1. Transient Stage

The creep curve of the transient strain is essentially given by the well-known equation [8]:

$$\varepsilon_{tr} = \beta t^{n} \qquad (1)$$

where ε_{tr} and t are the transient creep strain, and time, β and n are constants depending on the empirical experience states. The creep behaviour of the two tested solder alloys, is temperatures and stresses dependence i.e. increasing temperatures and stresses lead to increasing creep (strain with time), also the creep for Sn–9Zn-2Ag is higher than that of Sn-9Zn as presented in Fig. (1 a-e).

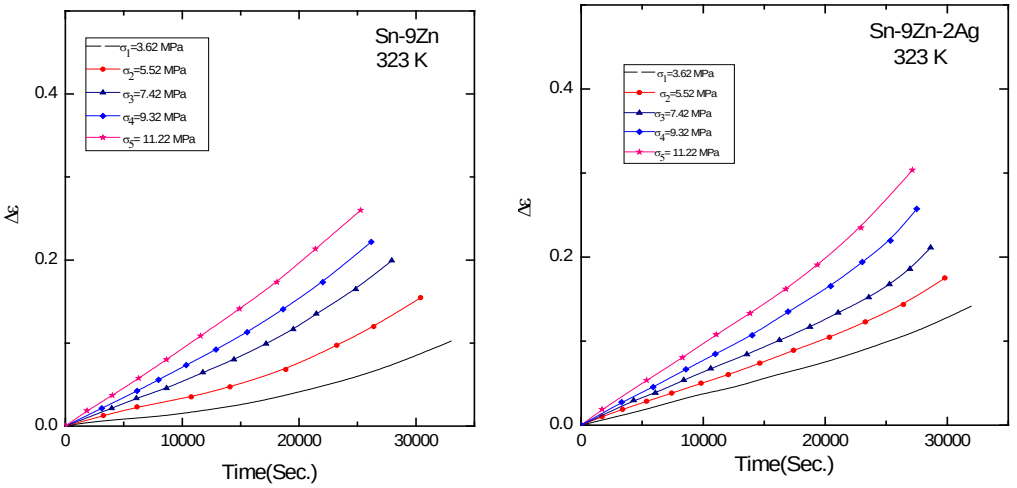

Fig.(1a): Isothermal Creep Curves at 323 K, at different applied stresses for Sn-9Zn eutectic and Sn-9Zn-2 A g alloys.

To compare the effect of small addition of Ag on Sn-9Zn lead-free solder alloys in the present study, Fig. (2) represented the creep curves of the two tested alloys at constant two stresses, 3.62 and 11.22 MPa and also two constant temperature, 323, and 403 K, it is obvious that the ternary Sn–9Zn-2Ag alloys is more superplastic than the binary in the two cases.

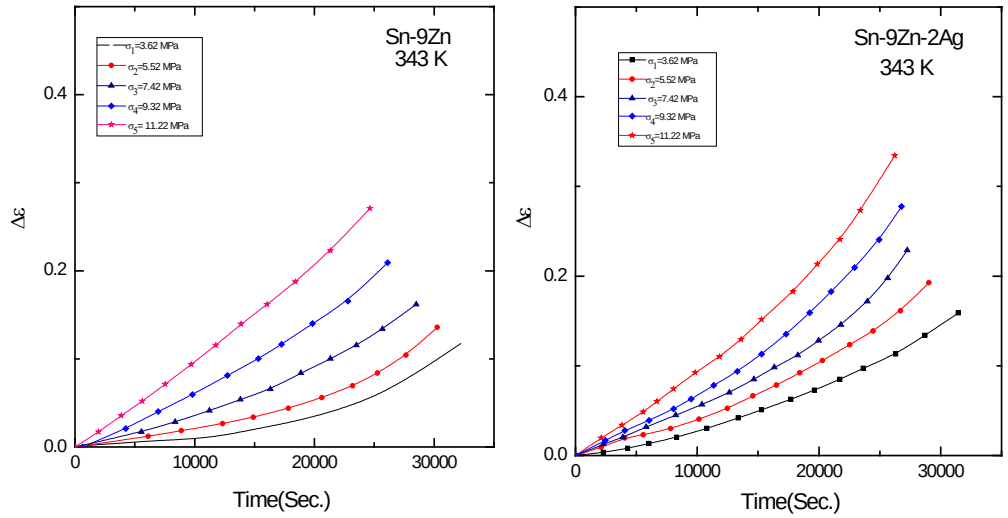

Fig.(1b): Isothermal Creep Curves at 343 K, at different applied stresses for Sn-9Zn eutectic and Sn-9Zn-2 A g alloys.

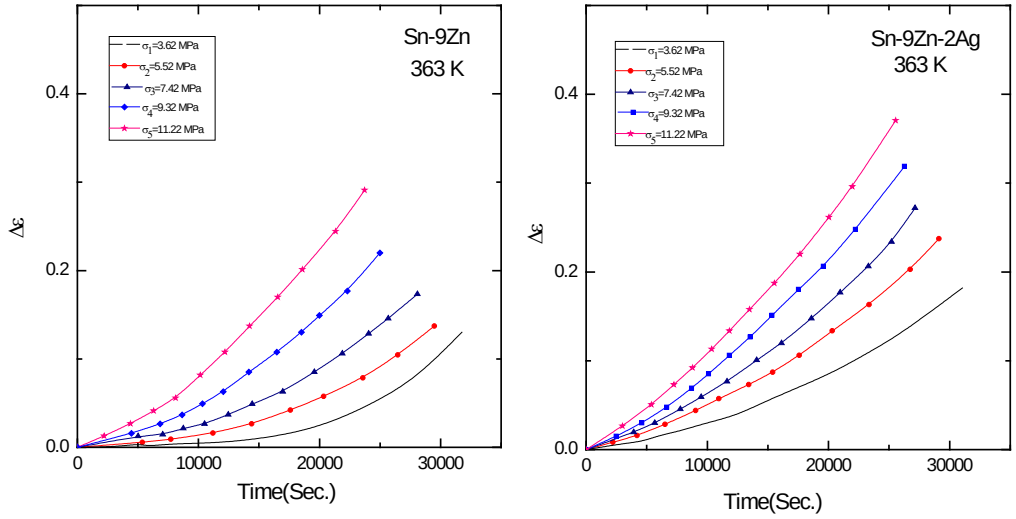

Fig.(1c): Isothermal Creep Curves at 363 K, at different applied stresses for Sn-9Zn eutectic and Sn-9Zn-2 A g alloys.

The creep curve at all the levels of applied stresses showed a rapid change from a small primary creep system, to a steady state and third creep regime. The relation between $\ln\varepsilon_{tr}$ and $\ln t$ gives straight lines as shown in Fig. (3 a-e). Slopes of these straight lines gave the values of the transient creep time exponent n and were found to have values ranging from 0.428 to 1.094 for Sn-9Zn binary alloy, and from 0.55 to 1.211 for Sn-9Zn-2Ag ternary alloys. It was found that n rises with rising deformation temperature for two alloys as in Fig.(4), while their intercepts at $\ln t = 0$ gave the transient creep parameter β; it was calculated from Eq.(2):

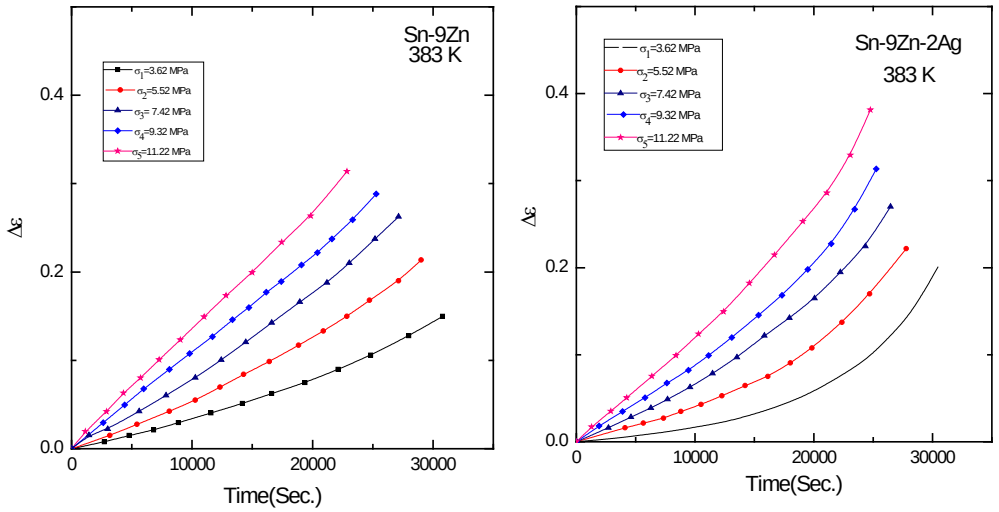

Fig.(1d): Isothermal Creep Curves at 383 K, at different applied stresses for Sn-9Zn eutectic and Sn-9Zn-2 A g alloys.

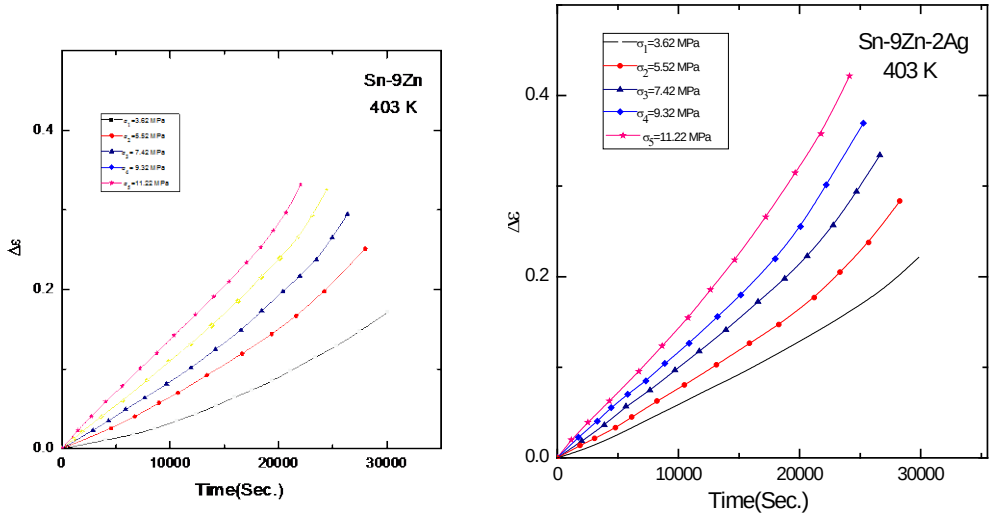

Fig.(1e): Isothermal Creep Curves at 403 K, at different applied stresses for Sn-9Zn eutectic and Sn-9Zn-2 A g alloys

$$\ln\beta = (\ln t_2\ \varepsilon_{tr1} - \ln t_1 \varepsilon_{tr2})/\ln t_2 - \ln t_1 \qquad (2)$$

The parameter β is raise with raising temperature and used stress as in Fig.(5), it was found to exhibit values ranging from -11.46 to -4.93 for Sn-9Zn binary alloy, and from -13.328 to -6.532 for Sn-9Zn-2Ag ternary alloys as shown in Table (2). Fig.(6) represents the relation between $\ln\varepsilon_{tr}$ and 1000/T at low temperature for Sn-9Zn eutectic and Sn-9Zn-2Ag alloys for different used stresses. These results yield activation enthalpies of 20.16 and 14.01 KJ/mole for Sn-9Zn eutectic and Sn-9Zn-2Ag in the low temperature regions. The activation

enthalpies for Sn-9Zn eutectic and Sn-9Zn-2Ag alloys were 28.82 and 20.22 KJ/mole in the high temperature regions as shown in Fig.(7). It is clear that activation enthalpies for Sn-9Zn binary alloys are more than ternary Sn-9Zn-2Ag alloys in low and high temperature section because of ternary alloys are smaller and fine in grain size and more in superplasticity than binary alloys.

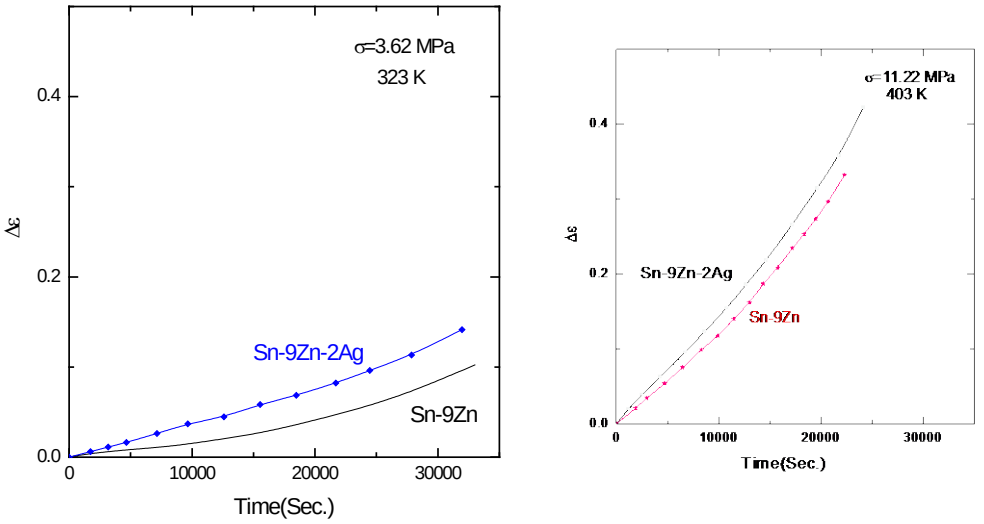

Fig.(2): Isothermal Creep Curves at 323 K and 403 K, at stresses 3.62 and 11.22 MPa for Sn-9Zn eutectic and Sn-9Zn-2Ag ternary alloys.

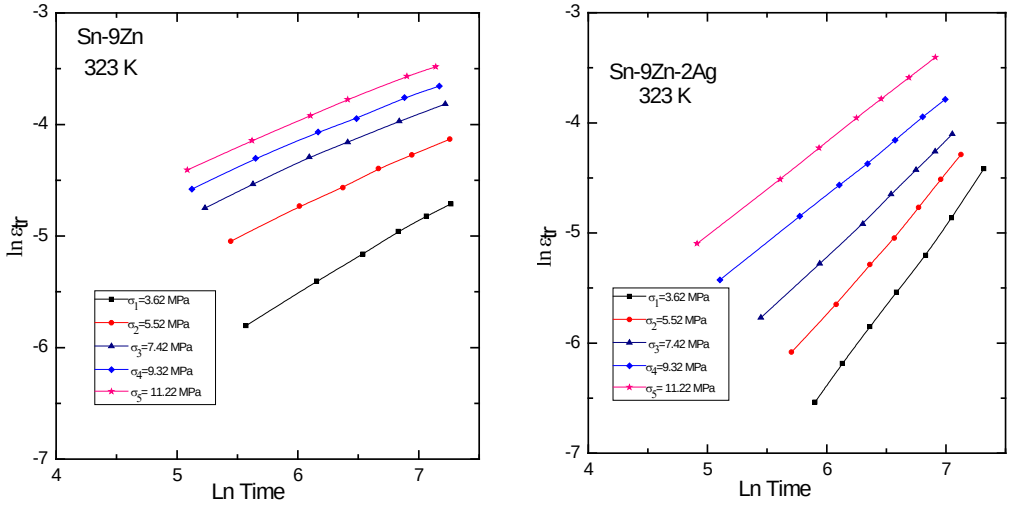

Fig.(3a): Relation between $\ln\varepsilon_{tr}$ and $\ln t$ for Sn-9Zn eutectic and Sn-9Zn-2Ag alloys, at 323K and different stresses.

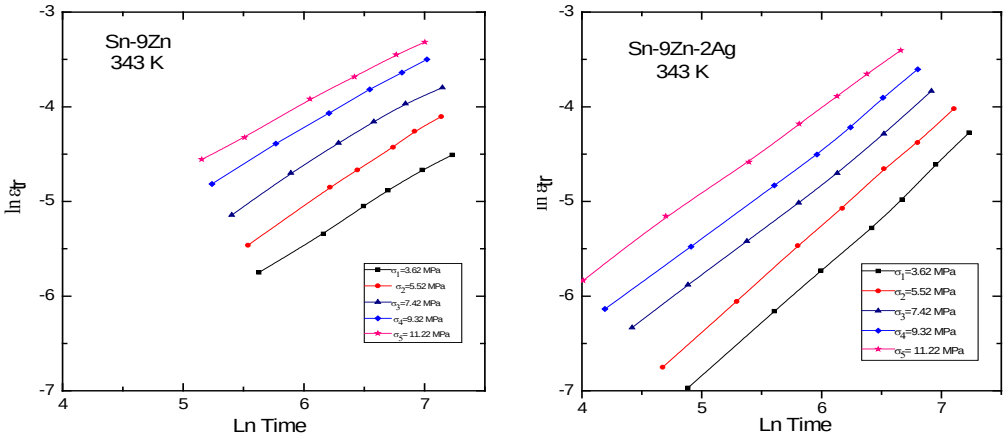

Fig.(3b): Relation between $\ln\varepsilon_{tr}$ and lnt for Sn-9Zn eutectic and Sn-9Zn-2Ag alloys, at 343K and different stresses.

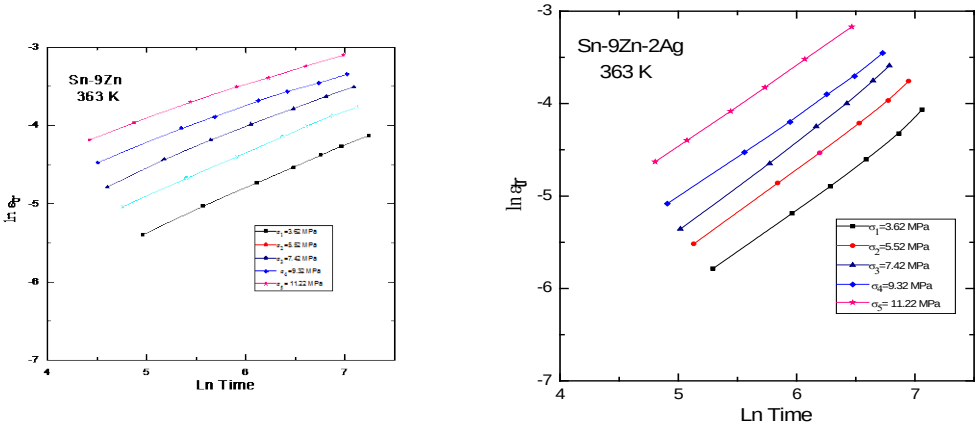

Fig.(3c): Relation between $\ln\varepsilon_{tr}$ and lnt for Sn-9Zn eutectic and Sn-9Zn-2Ag alloys, at 363K and different stresses.

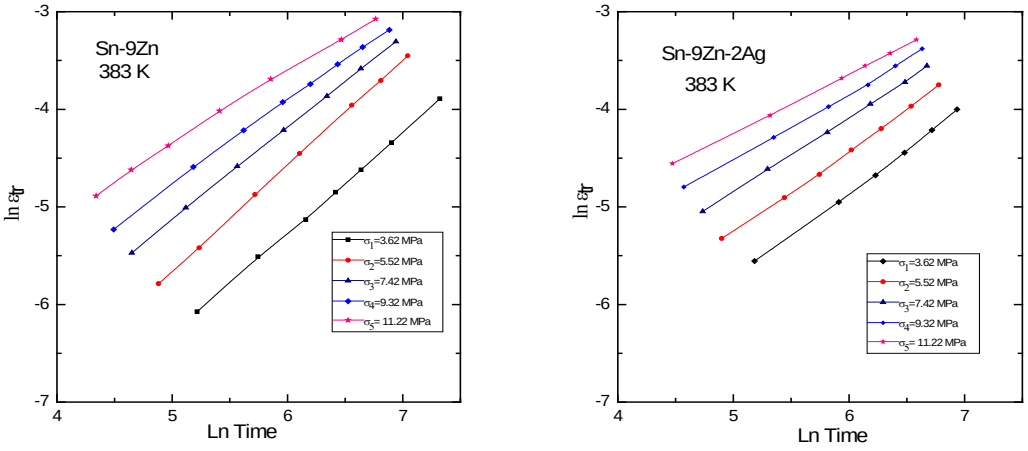

Fig.(3d): Relation between $\ln\varepsilon_{tr}$ and lnt for Sn-9Zn eutectic and Sn-9Zn-2Ag alloys, at 383K and different stresses.

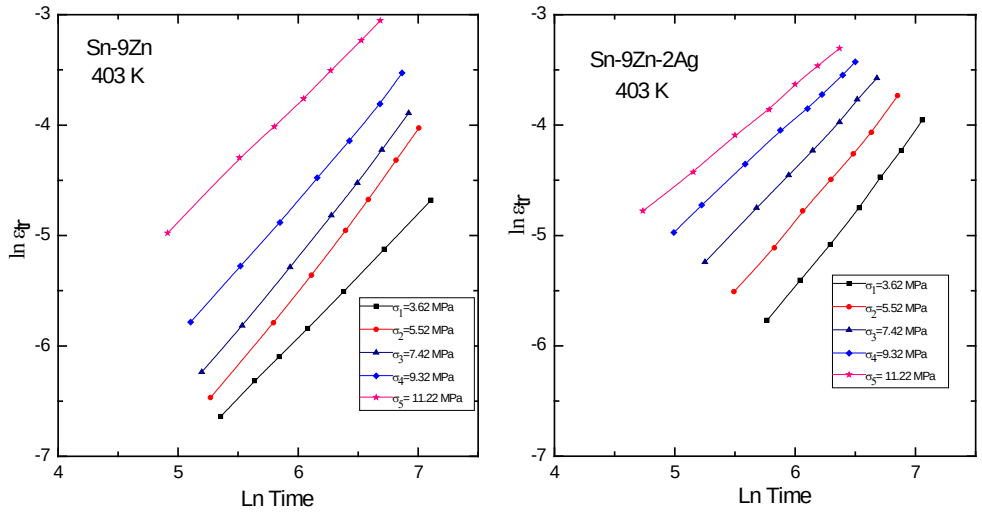

Fig.(3e): Relation between $\ln\varepsilon_{tr}$ and lnt for Sn-9Zn eutectic and Sn-9Zn-2Ag alloys, at 403K and different stresses.

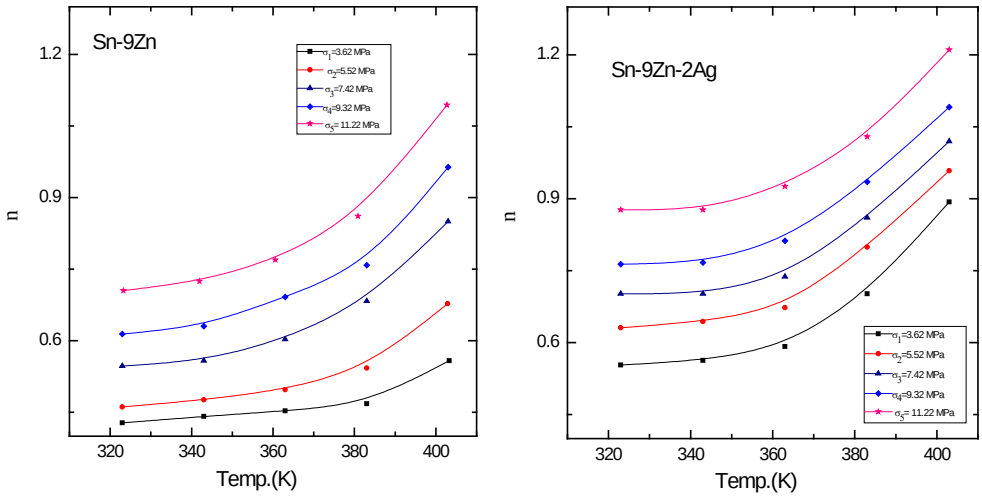

Fig.(4): The dependence of the parameters, n, on the working temperature at different applied stresses for Sn-9Zn eutectic and Sn-9Zn-2 A g alloys.

Table (2): Comparison of the transient creep characteristics of the tested alloys.

material	n	β	Q (kJmol-1)
Sn-9Zn	0.428 : 1.094	-11.46 : -4.93	20.16 : 28.82
Sn-9Zn-2Ag	0.55 : 1.211	-13.328 : -6.53	14.01 : 20.22

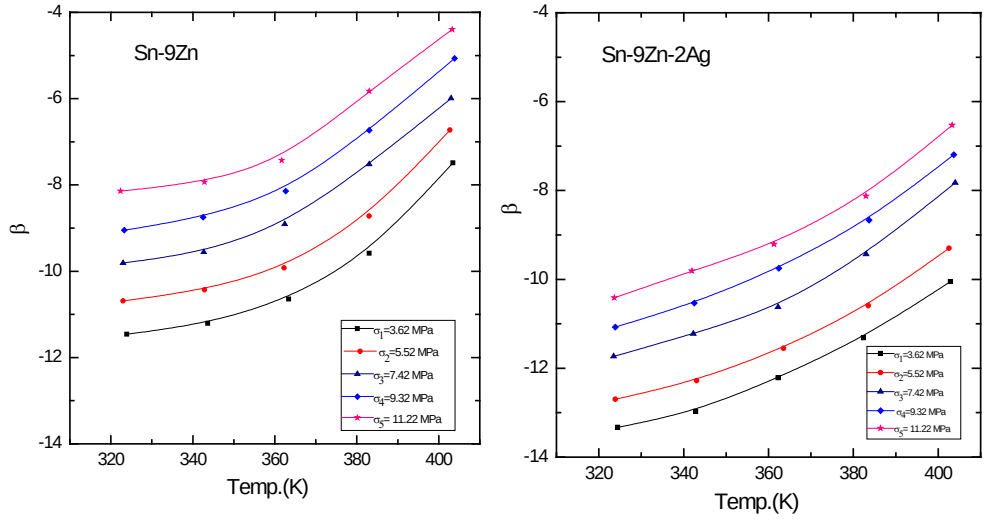

Fig.(5): The dependence of the parameters, β, on the working temperature at different applied stresses for Sn-9Zn eutectic and Sn-9Zn-2 A g alloys.

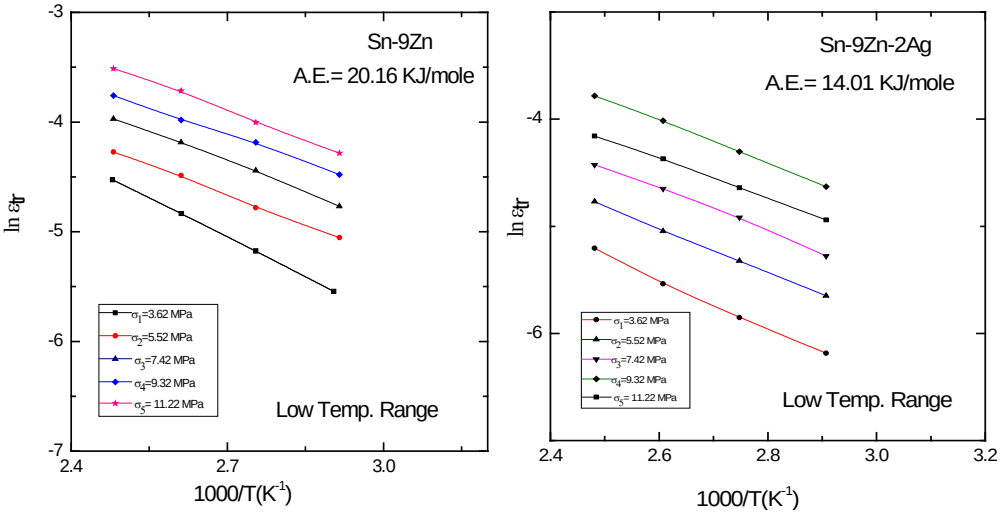

Fig.(6): The relation between $Ln\varepsilon_{tr}$ and 1000/T at different applied stresses for Sn-9Zn eutectic and Sn-9Zn-2 A g alloys at low Temp.

3.1.2. Steady-State Creep Stage

The steady-state strain rate ε´st of the used specimen is calculated from the slopes of the linear parts of the creep curves presented in Fig.(1). It rises with raising the temperature and stress in used alloys as seen in Fig.(8). It can be seen that under the same test conditions the ternary alloy exhibited higher strain rate ε´st with respect to that of the binary one. It can be seen that each curve is

described by all the three characteristic regions: (I) primary, (II) secondary or steady state, and (III) tertiary. Since the stress and temperature are stables, the difference in creep rates, $\dot{\varepsilon}$, proposes a requisite change in the internal structure of the alloy through time. The strain ε and strain rate $\dot{\varepsilon}$ are, in general, lower for Sn-9Zn eutectic samples than for Sn-9Zn-2Ag samples in spite of the applied stress and temperature.

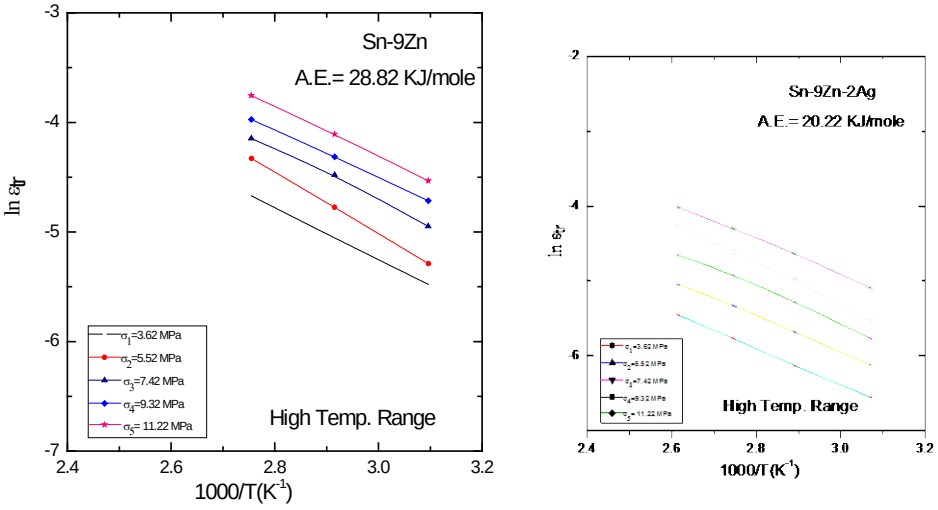

Fig.(7): The relation between Lnε_{tr} and 1000/T at different applied stresses for Sn-9Zn eutectic and Sn-9Zn-2 A g alloys at high Temp.

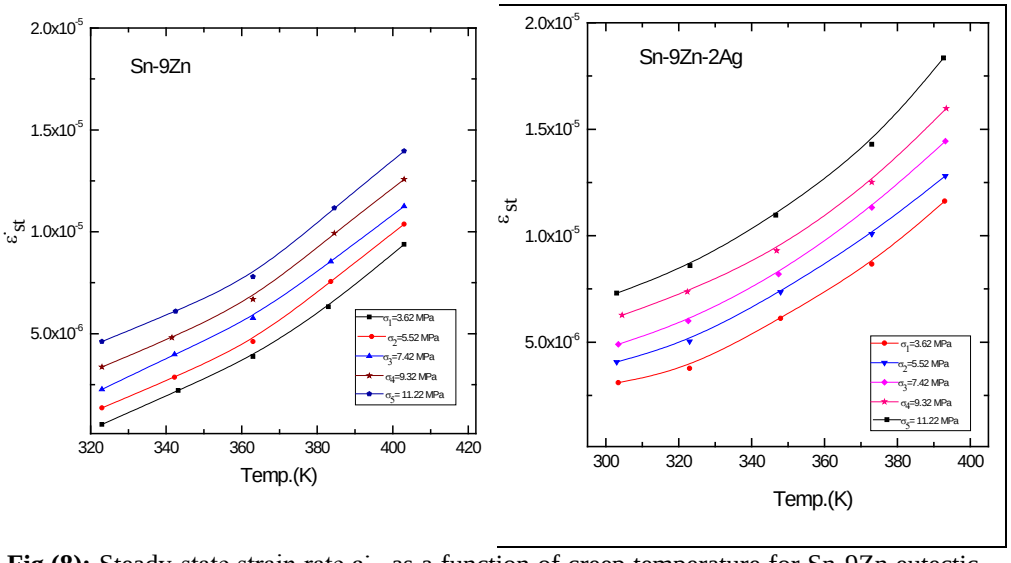

Fig.(8): Steady-state strain rate $\dot{\varepsilon}_{st}$ as a function of creep temperature for Sn-9Zn eutectic and Sn-9Zn-2 A g alloys.

Such distinctions in the creep manner may be related to the variation in the grain size of the two alloys. At low creep rate no temperature dependence of strain, suggests that the creep behaviour is strongly affected by the Ag-addition. Moreover, the obtained lower creep rates are not influenced by the creep weakening factor of dynamic recrystallization [9].

The differences in creep rate, $\dot{\varepsilon}$, suggest a necessary variation in the internal resistance stress of the used sample during time. This proposes that the hardening of the matrix was recovered at once and fixed at an expanded deformation rate [3].

However, additions of Ag resulted in increasing the creep rates. The Sn-9Zn alloys showed a minimum creep rate than Sn-9Zn-2Ag. The observed increase in creep rates ($\dot{\varepsilon}$) with Ag-additions suggests that the creep behaviour of Sn-9Zn-2Ag is mainly affected by the new Ag_3Sn IMCs formed in the ternary alloys. The existence of Ag_3Sn IMCs particles may influence the distance that dislocations glide through obstacles and the forces that produce them to climb. Furthermore, there are some activated processes may take place in particle hardened alloys such as particle by pass by dislocation climb and favourite interactions in dislocations and particles that do not take place in fine materials. Thus, it is confirm that the increase in creep rates ($\dot{\varepsilon}$) with Ag additions happens as a result of variation in particle by-pass mechanism.

Since the lead- free Sn-9Zn-2Ag solder shows superior creep performance over the binary Sn-9Zn solders in terms of much higher creep behaviour and vastly elongated creep fracture lifetime, moreover, grain size refinement plays a role to increase the creep rate of solders, since its large grain boundary areas act as a barrier for pinning the dislocation movement. An identical reliance was set up by Wu et al. [10]. The present work informed that the lower in grain size minimize the stress intensity at grain boundaries and, thus, retards cavity nucleation. Thus, the superfine grain size of β-Sn and more uniform dispersion of IMCs particles were the main reasons for the improvement of strain. Nonetheless, Mahmudi et al. [11] Showed that this grain refinement should not be considered as the main cause of better strain in the more concentrated alloys. Instead, it is then softening mechanisms of Ag3Sn IMCs in the β -Sn matrix which are responsible for the observed improvement in creep behaviour.

The variation of the transient creep parameter $\ln\sigma$, (where σ is the stress in MPa) with the steady state creep $\ln\dot{\varepsilon}_{st}$ for different applied stresses for Sn-9Zn eutectic and Sn-9Zn-2Ag alloys as in Fig.(9). The value of strain rate sensitivity parameter m calculated from the slopes of these straight lines, and was found to have values ranging from 0.24 to 0.356 for Sn-9Zn binary alloy, and from 0.31 to 0.44 for Sn-9Zn-2Ag ternary alloys as shown in Fig.(10). It is shown that the value of m for Sn-9Zn-2Ag ternary alloys is higher than that of Sn-9Zn binary alloy, illustrating that the sensitivity parameter m for both compositions is temperature and strain dependent i.e. sensitivity parameter increases with temperature and strain.

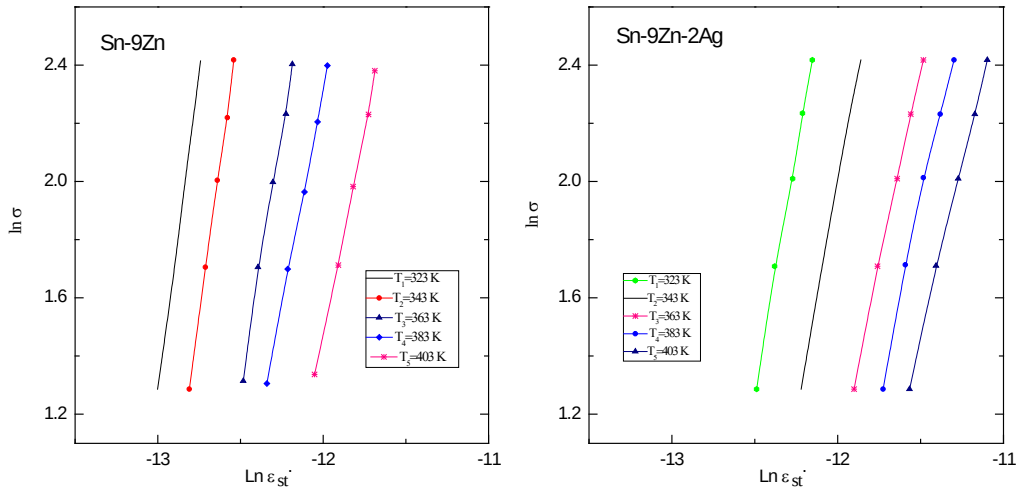

Fig.(9): Strain rate–stress relationship for for Sn-9Zn eutectic and Sn-9Zn-2Ag alloys.

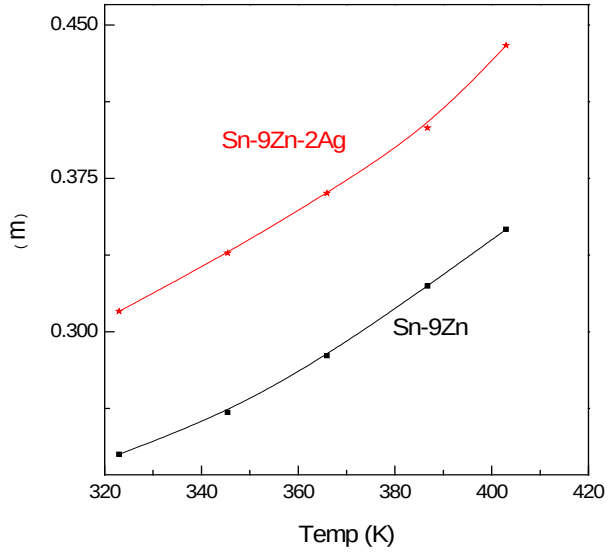

Fig.(10): Strain rate sensitivity parameter m as a function of creep temperature Sn-9Zn eutectic and Sn-9Zn-2Ag alloys.

The activation energy of steady creep at fixed loads was studied utilizing equation [12].

$$Q = R\left(\partial \ln \varepsilon_{st} / \partial\left(1/T\right)\right) \tag{3}$$

where R and T are the gas constant and temperature in K. Moreover, the obtained results verify the equation of steady state creep [18-20]

$$\varepsilon \cdot_{st} = c\left(\frac{\sigma}{d}\right)^{1/m} \exp\left(\frac{Q}{kT}\right) \tag{4}$$

where m = 0.5 for dislocation climb through grain boundaries [13] therefore, it is believed here that the great elongation is assigned to the dislocation movement product in grain boundary sliding (*GBS)* and contained it during the deformation. The activation energy of steady state creep was calculated from the relation between $\ln\dot{\varepsilon}_{st}$ and 1000/T at low and high temperature for Sn-9Zn eutectic and Sn-9Zn-2Ag alloys used applied stresses. The activation energies for the binary eutectic and ternary alloys have been found to be 21.99-24.73 and 15.13-22.07 kJ/mole in the low and high temperature zones, respectively in Fig.(11, 12). It is obvious that activation enthalpies for Sn-9Zn binary alloys are more than ternary Sn-9Zn-2Ag alloys in low and high temperature regions see Table (3).

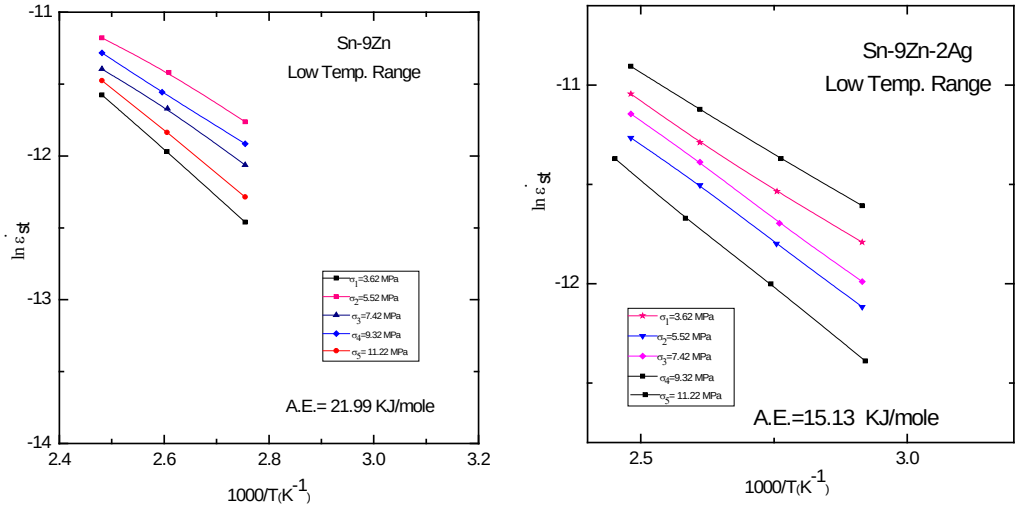

Fig.(11): The relation between $\ln\varepsilon_{tr}$ and 1000/T at different applied stresses for Sn-9Zn eutectic and Sn-9Zn-2 A g alloys at low Temp.

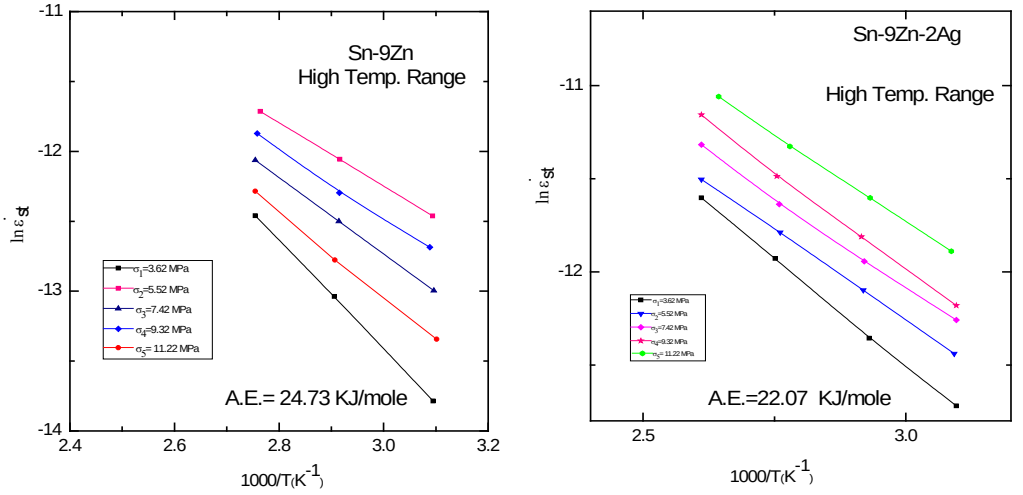

Fig.(12): The relation between $\ln\varepsilon_{tr}$ and 1000/T at different applied stresses for Sn-9Zn eutectic and Sn-9Zn-2 A g alloys at low Temp.

Table (3): Comparison of the steady state creep characteristics of the tested alloys.

material	m	ε'_{st}	Q (kJmol-1)
Sn-9Zn	0.24 : 0.356	$5.52*10^{-7} : 1.39*10^{-5}$	21.99 : 24.73
Sn-9Zn-2Ag	0.31 : 0.44	$3*10^{-6} : 1.84*10^{-5}$	15.13 : 22.07

According to the Sn-Zn binary phase diagram see Fig.(13), the equilibrium microstructure of the eutectic Sn-9Zn constitutes of the eutectic combine of Sn-rich (near to pure Sn) phase and the Zn-rich phase. Addition of 2Ag to binary alloys form the respective ternary Sn-9Zn-2Ag solder alloy which are much higher (more superplastic) than those of the binary [14].

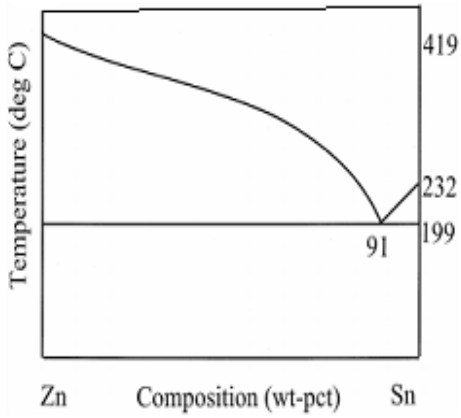

Fig.(13): Phase diagram for Sn-9Zn binary system.

The OM images of the two alloys are given in Fig.(14). In Fig.(14a), a typical eutectic Sn-9Zn microstructure composed of light gray areas of Sn_5Zn_8 IMCs and dark network-like eutectic regions of β-Sn grain boundaries. In Fig.(14b), the appropriate content of Ag in the Sn-9Zn solder was found to improve the microstructure of the alloy. The primary Ag_3Sn IMCs might act as heterogeneous nucleation sites for β-Sn dendrites upon solidification and are able to refine the grain size of Sn-9Zn alloy. Consequently, the mechanical properties of Sn-9Zn-2Ag solder may be enhanced.

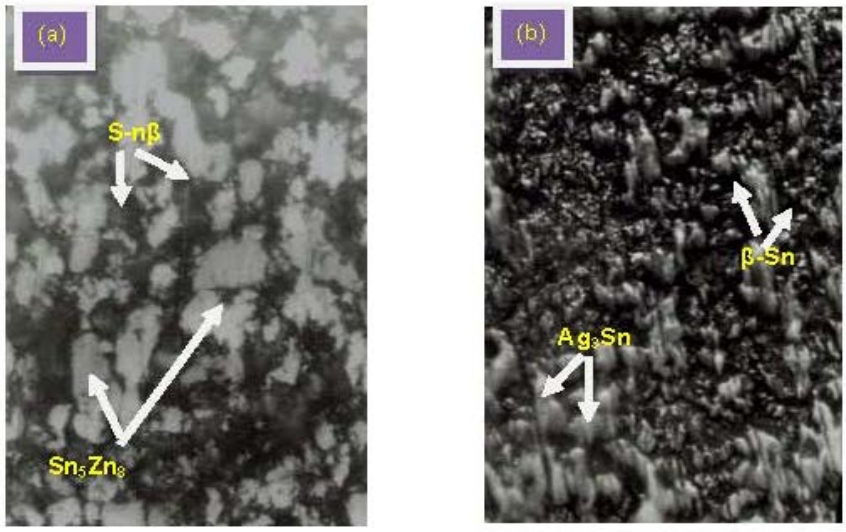

Fig.(14): The OM images of the two alloys (a) a typical eutectic Sn–9Zn microstructure composed of light gray areas of Sn_5Zn_8 IMCs and dark network-like eutectic regions of β-Sn grain boundaries. In (b), the appropriate content of Ag in the Sn-9Zn solder was found to improve the microstructure of the alloy. The primary Ag_3Sn IMCs might act as heterogeneous nucleation sites for β-Sn dendrites upon solidification and are able to refine the grain size of Sn-9Zn alloy, the microstructure in the ternary alloys must be uniform and finer grain size.

Fig.(15) displayed the XRD conclusion of the as-cast Sn-9Zn and Sn-9Zn-2Ag experimental alloys. In general, all the as-cast experimental alloys are mainly composed of β-Sn phase and precipitated Sn_5Zn_8 phase. However, the alloys containing Ag exhibited additional IMCs such as Ag_3Sn.

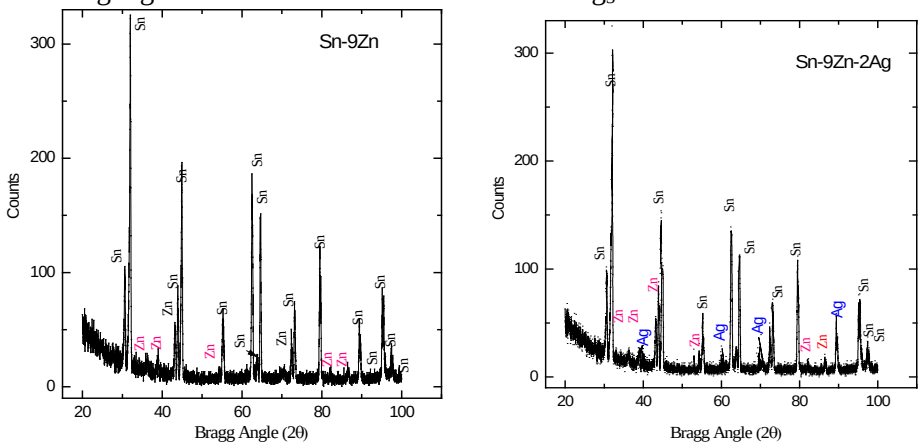

Fig.(15): (a) XRD pattern for Sn-9Zn binary alloy are mainly composed of β-Sn phase and precipitated Sn_5Zn_8 phase and, (b) Sn-9Zn-2Ag ternary alloys containing Ag exhibited additional IMCs such as Ag_3Sn.

It is obvious that the Sn-9Zn alloy has two types of precipitates having various morphologies. The first one has a constant network and the latest has an isolated thin particles-like shape. According to the XRD the continuous precipitates are β-sn, phases while the fine particle precipitates are Sn_5Zn_8 IMCs. It is remarkable to note from Fig.14(b) that with adding 2Ag to the Sn-9Zn alloy, the morphology of the Sn_5Zn_8 phase in the alloy gradually changes from coarse polygonal precipitates to a relatively fine quasi-continuous disconnected shape Ag_3Sn. Despite the high content of tin (because the matrix of the solder was β-Sn), the fine particles should be Ag_3Sn IMCs.[15].

Conclusion

This paper has inspected the effectiveness of small amount of Ag on microstructure and creep properties of Sn-9Zn based lead-free solder alloys. The conclusions are:

1- The transient creep parameter *n*, β, strain rate sensitivity parameter m, and steady-state strain rate $\dot{\varepsilon}_{st}$ all are increase with increasing the deformation temperature, and stress their values in case of Sn-9Zn-2Ag are more than that of Sn-9Zn

2- It is clear that activation enthalpies for Sn-9Zn binary alloys are higher than ternary Sn-9Zn-2Ag alloys for transient and steady state creep regions, therefore ternary alloys show higher strain than Sn-9Zn binary eutectic.

3. From microstructure examination, the coarse Sn_5Zn_8 IMCs are precipitated within the β-Sn matrix in the Sn-9Zn based lead-free solder alloys. The Sn-9Zn-2Ag ternary alloys exhibited additional constituent phases of Ag_3Sn IMCs.

References

1. A.A. El-Daly, A.Z. Mohamad, A. Fawzy, A.M. El-Taher, *Materials Science and Engineering*, A **528**, 1055 (2011).

2. R.M. Shalaby, *J. Alloys Compd*., **480**, 334 (2009).

3. A.A. El-Daly, Y. Swilem, A.E. Hammad, *J. Alloys Compd*., **471**, 98 (2009).

4. M. Loomans, S. Vaynman, G. Ghosh, M. Fine, *J. Electron. Mater*., **23**, 741 (1994).

5. J. Corbin IBM, *J. Res. Develop*., **37**, 585 (1993).

6. R. Mahmudi, A.R. Geranmayeh, A. Rezaee-Bazzaz, *Mater. Sci. Eng*. A **448**, 287 (2007).

7. A.A. El-Daly, Y. Swilem, A.E. Hammad, *J. Mater. Sci. Technol*., **24**, 921 (6) (2008).

8. J. Friedel, *Dislocations, Pergamon Press, London*, p. 304 (1964).

9. O. Takahashi, Y. Terada, M. Takeyama, T. Matsuo, *Mater. Sci. Eng*., A **329**, 835 (2002).
10. C.M.L. Wu, D.Q. Yu, C.M.T. Law, L. Wang, *J. Electron. Mater*., **31**, 928 (2002).
11. R. Mahmudi, A.R. Geranmayeh, A. Rezaee-Bazzaz, *Mater. Sci. Eng*., A **448**, 287 (2007).
12. J.Weertman, *Rate Processes in Plastic Deformation of Materials*, **315** (ASM, 1975).
13. A.A. El-Dalya, A.Z. Mohamad, A. Fawzy, A.M.El-Taher, *Materials Science and Engineering*, A **528**, 1055 (2011).
14. Hucheng Pan, He Fu, Yuping Ren, Qiuyan Huang, Zhengyuan Gao, Jia She, Effect of Cu/Zn on microstructure and mechanical properties of extruded Mg–Sn alloys, *Mater. Sci. Technol*, **32**,1240 (2016).
15. C. Wei, Y. Liu, Z. Gao, R. Xu, K. Yang, *J. Alloys Compd*., **468**, 154 (2009).